University of Zurich[UZH]

Institute of Physics

Master Thesis

Electroweak Sudakov Logarithms in Vector Boson + Jet Production

Niklaus Häfliger

Supervisors: Prof. Dr. Stefano Pozzorini
Dr. Jonas Lindert

January 2016

Contents

List of Figures

1. Introduction

The production of a vector boson in association with jets represents one of the most prominent classes of processes studied at the Large Hadron Collider (LHC). Thanks to the large cross section and clean experimental signature, vector boson + jet production can be probed with high accuracy over a wide range of jet multiplicities and energy scales [1–6]. Such measurements provide a powerful testing ground for the Standard Model as well as for perturbative QCD methods and tools that build the fundament of all theoretical simulations of high-energy collisions at hadron colliders.

Moreover V + multijet production is the dominant background in several searches of physics beyond the Standard Model (BSM) that are based on signatures with leptons, missing energy, and jets. In this context, precise theoretical predictions of the V + multijet (V=W,Z) background can play a critical role for the precision of the measurements and the sensitivity to new phenomena.

Predictions for V + multijet production at next-to-leading order (NLO) in QCD have been available for some time, and even reach next-to-next-to-leading order (NNLO) precision for V + 1 jet [7, 8].

Including the electroweak (EW) NLO corrections has proved more difficult due to the presence of massive particles whose mass can not be neglected without sacrificing precision. While NLO predictions for V + 1 jet have been available for a while, V + multijet calculations have only become possible recently due to advances in the automation of NLO calculations. [9–14]

Focusing on the more feasible QCD corrections and neglecting the EW corrections can be justified for the calculation of integrated cross sections, where the QCD effects dominate EW effects due to the difference between α_s (~ 0.12) and α (~ 0.008). However, depending on the phase space region highlighted by a particular differential cross section, EW corrections can become very significant.

Precise predictions for pp $\to$ V + n jets are not only obviously important for observables that involve at least n jets, but they also play an important role for inclusive observables that allow, but do not explicitly require, several jets. Important examples are the inclusive distribution in the transverse momentum (p_T) of the leading jet and the total transverse energy. As a result, NLO QCD predictions for pp $\to$ V + 1 jet at high jet p_T are plagued by giang K-factors and large scale uncertainties due to the dominance of n-jet final states with $n \geq 2$. It is clear that it is also not enough to include NLO EW results for pp $\to$ V + 1 jet only as they also miss the dominant effects, namely Sudakov-type EW corrections to V + multijet production.

Having a computationally feasible method of calculating NLO EW corrections to V + multijet production for as many jets as possible would therefore be a very desirable remedy to the situation. The EW Sudakov approximation (applicable at high energy colliders such as the LHC when all hard-scattering energy parameters are well above the EW scale) is one such method and it is a goal of this thesis to compare it's predictions to the full NLO EW corrections.

One key motivation of this work is to test the validity of the Sudakov approximation for the case of V+multijet final states by comparing the results to the recent exact

calculations of NLO EW mentioned above. If the Sudakov approximation can be validated as a close approximation, it would become a very powerful tool for obtaining NLO EW results for final states involving many particles.

2. Electroweak (EW) Sudakov Logarithms as an Approximation of NLO EW corrections

The derivation of the analytical expressions for the EW Sudakov logarithms was the subject of reference [15]. This section provides a short summary of the formulas relevant to the implementation.

We use the convention that all n external particles and their momenta are incoming, such that the process reads

$$\varphi_{i_1}(p_1)\dots\varphi_{i_n}(p_n)\to 0 \tag{2.1}$$

and four momentum conservation requires that

$$\sum_{k=1}^{n} p_k = 0. \tag{2.2}$$

Predictions for general processes with in- and outgoing particles can be obtained by crossing symmetry.

All external particles are considered to be on-shell, i.e. $p_k^2 = M_k^2$.

We restrict ourselves to the kinematic region where all invariants r_{kl} are much larger than the gauge boson masses:

$$r_{kl} = (p_k + p_l)^2 \gg M_W^2 \tag{2.3}$$

This condition is satisfied if the center-of-mass energy $\sqrt{s} \gg M_W$ and the scattering angles are not too small.

The Sudakov approximation of NLO EW corrections captures all terms that are logarithmically enhanced, i.e. terms that involve one or two powers of $\log(\hat{s}/M^2)$. Correction terms of order α that do not grow with increasing energy are neglected.

The logarithmic approximation of the virtual one-loop corrections lead to double (DL) and single (SL) logarithmic terms written in terms of

$$L(r_{kl}, M^2) := \frac{\alpha}{4\pi}\log^2\frac{|r_{kl}|}{M^2}, \quad l(r_{kl}, M^2) := \frac{\alpha}{4\pi}\log\frac{|r_{kl}|}{M^2}, \tag{2.4}$$

depending on the invariants r_{kl} as defined in (2.3) and masses M.

We will be able to write the corrections in the form

$$\delta = \delta^{\mathrm{LSC}} + \delta^{\mathrm{SSC}} + \delta^{\mathrm{C}} + \delta^{\mathrm{PR}}, \tag{2.5}$$

where the DL corrections make up the leading soft-collinear (LSC) and subleading soft-collinear (SSC) contributions, while the SL corrections form the contributions due to soft or collinear (C) gauge boson emission and parameter renormalization (PR).

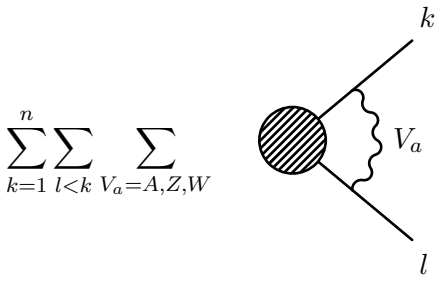

Figure 1: Feynman diagrams leading to DL corrections (external legs not involved in exchange not shown)

The DL corrections originate from loop diagrams where virtual gauge bosons V_a = A,Z,W$^\pm$ are exchanged between pairs of external legs (Figure 1). The double logarithms arise from the integration region where the gauge-boson momenta are soft and collinear to one of the external legs.

By evaluating these diagrams in the eikonal approximation, where in the numerator of the loop integral the gauge boson momentum is set to zero and all mass terms are neglected, and using the high-energy expansion of the scalar three-point function, one obtains

$$\delta\mathcal{M}^{i_1\dots i_n} = \frac{1}{2}\sum_{k=1}^{n}\sum_{l\neq k}\sum_{V_a=A,Z,W^\pm} I^{V_a}_{i'_k i_k}(k) I^{\bar{V}_a}_{i'_l i_l}(l)\mathcal{M}_0^{i_1\dots i'_k\dots i'_l\dots i_n} L(|r_{kl}|, M^2_{V_a}). \tag{2.6}$$

Using

$$\log^2\left(\frac{|r_{kl}|}{M^2}\right) = \log^2\left(\frac{s}{M^2}\right) + 2\log\left(\frac{s}{M^2}\right)\log\left(\frac{r_{kl}}{s}\right) + \log^2\left(\frac{r_{kl}}{s}\right), \tag{2.7}$$

we can expand (2.6) in terms of $\log(s/M^2_W)$. The angular dependent part is contained in logarithms of r_{kl}/s. The term $\log^2(r_{kl}/s)$ we neglect in LA. The other logarithms are angular independent and give the leading soft-collinear (LSC) contribution.

Using the fact that the S matrix is invariant with respect to global SU(2) $\times$ U(1) transformations, which implies

$$\sum_{l\neq k} I^{V_a}(l) = -I^{V_a}(k), \tag{2.8}$$

the LSC corrections can be written as

$$\delta^{\mathrm{LSC}}(k) = -\frac{1}{2}\left[C^{\mathrm{ew}}_{i'_k i_k}(k)L(s) - 2(I^Z(k)_{i'_k i_k})^2\log\frac{M_Z^2}{M_W^2}l(s) + \delta_{i'_k i_k}Q_k^2 L^{\mathrm{em}}(s,\lambda^2,m_k^2)\right], \tag{2.9}$$

where $C^{\mathrm{ew}}_{i'_k i_k}$ denotes the EW Casimir operator

$$C^{\mathrm{ew}}_{i'_k i_k} = \sum_{V_a = A,Z,W^\pm} I^{V_a}_{i'_k i_k} I^{\bar{V}_a}_{i'_k i_k}, \tag{2.10}$$

and the last term contains the purely electromagnetic contribution with Q_k being the electromagnetic charge of particle k and

$$L^{\mathrm{em}}(s, \lambda^2, m_k^2) := 2l(s) \log\left(\frac{M_W^2}{\lambda^2}\right) + L(M_W^2, \lambda^2) - L(m_k^2, \lambda^2). \tag{2.11}$$

Explicit values for C^{ew} can be found in appendix A.

The subleading soft-collinear contribution to (2.6) remains a sum over pairs of external legs with angular-dependent terms.

$$\delta^{\mathrm{SSC}} \mathcal{M}^{i_1 \dots i_n} = \sum_{k=1}^{n} \sum_{l<k} \sum_{V_a = A,Z,W^\pm} \delta^{V_a,\mathrm{SSC}}_{i'_k i_k i'_l i_l}(k,l) \mathcal{M}_0^{i_1 \dots i_k \dots i'_l \dots i_n} \tag{2.12}$$

The exchange of gauge bosons contributes with

$$\begin{aligned}
\delta^{A,\mathrm{SSC}}_{i'_k i_k i'_l i_l}(k,l) &= 2\left[l(s) + l(M_W^2, \lambda^2)\right] \log\left(\frac{|r_{kl}|}{s}\right) I^A_{i'_k i_k}(k) I^A_{i'_l i_l}(l), \\
\delta^{Z,\mathrm{SSC}}_{i'_k i_k i'_l i_l}(k,l) &= 2l(s) \log\left(\frac{|r_{kl}|}{s}\right) I^Z_{i'_k i_k}(k) I^Z_{i'_l i_l}(l), \\
\delta^{W^\pm,\mathrm{SSC}}_{i'_k i_k i'_l i_l}(k,l) &= 2l(s) \log\left(\frac{|r_{kl}|}{s}\right) I^\pm_{i'_k i_k}(k) I^\pm_{i'_l i_l}(l),
\end{aligned} \tag{2.13}$$

where the couplings are diagonal matrices for the neutral gauge bosons A and Z. The exchange of W bosons leads to the appearance of SU(2)-transformed matrix elements on the right-hand side of (2.12). These are in general related to the original Born matrix element in a nontrivial way.

The single logarithms (SL) originate from field renormalization and from mass-singular loop diagrams (δ^{C}) as well as from parameter renormalization (δ^{PR}).

Field renormalization gives the well-known factors $\delta Z_\varphi/2$ for each external leg, which contain collinear as well as soft SL contributions.

$$\delta^{\mathrm{C}}_{i'_k i_k}(k) = \delta^{\mathrm{coll}}_{i'_k i_k}(k) + \frac{1}{2} \delta Z^{\varphi}_{i'_k i_k} \Big|_{\mu^2 = s}. \tag{2.14}$$

For chiral fermions, the non-negligible contribution to δ^{C} reads

$$\delta^{\mathrm{C}}_{f_\sigma f_{\sigma'}}(f^\kappa) = \delta_{\sigma\sigma'} \frac{3}{2} C^{\mathrm{ew}}_{f^\kappa}, \tag{2.15}$$

and for transverse gauge bosons (V_T) it is

$$\begin{aligned}
\delta^{\mathrm{C}}_{W^{\sigma\sigma'}}(V_T) &= \delta_{\sigma\sigma'}\frac{1}{2}b^{\mathrm{ew}}_W l(s),\\
\delta^{\mathrm{C}}_{AA} &= \frac{1}{2}b^{\mathrm{ew}}_{AA} l(s),\\
\delta^{\mathrm{C}}_{ZZ} &= \frac{1}{2}b^{\mathrm{ew}}_{ZZ} l(s),\\
\delta^{\mathrm{C}}_{AZ}(V_T) &= b^{\mathrm{ew}}_{AZ} l(s),\\
\delta^{\mathrm{C}}_{ZA}(V_T) &= 0,
\end{aligned} \tag{2.16}$$

where b^{ew} denotes the one-loop coefficient of the β-function.

The SL originating form the renormalization of the parameters e (electric charge), c_w (cosine of the weak mixing angle) and the mass ratios $h_t = \frac{m_t}{M_W}$ and $h_H = \frac{M_H^2}{M_W^2}$ is

$$\delta^{\mathrm{PR}}\mathcal{M} = \frac{\delta\mathcal{M}_0}{\delta e}\delta e + \frac{\delta\mathcal{M}_0}{\delta c_w}\delta c_w + \frac{\delta\mathcal{M}_0}{\delta h_t}\delta h_t + \frac{\delta\mathcal{M}_0}{\delta h_H}\delta h_H^{\mathrm{eff}}\Bigg|_{\mu^2=s}. \tag{2.17}$$

For the relevant counterterms for the implementation of V+multijet are the ones for the electric charge and the weak mixing angle:

$$\begin{aligned}
\frac{\delta c_w^2}{c_w^2} &= \frac{s_w}{c_w}b^{\mathrm{ew}}_{AZ} l(\mu^2)\\
\delta Z_e &= -\frac{1}{2}b^{\mathrm{ew}}_{AA} l(\mu^2) + \delta Z_e^{\mathrm{ew}}\\
\delta Z_e^{\mathrm{ew}} &= \frac{2}{3}\sum_{f,i,\sigma\neq t} N_C^f Q_{f_\sigma}^2 l(M_W^2, m^2_{f_{\sigma,i}})
\end{aligned} \tag{2.18}$$

This gives us all the ingredients needed for implementing the EW Sudakov corrections to V + multijet production.

3. Implementation

The EW Sudakov logarithms have been implemented using the existing software programs `OpenLoops` [14], `Sherpa` [16] and `Rivet` [17]. `Sherpa` is a fully featured Monte Carlo event generator and is used as the main program controlling the calculations. `OpenLoops` provides matrix elements and can be used as a plug-in to `Sherpa`. Finally, `Rivet` is used for analyzing the generated events and creating the desired histograms.

`OpenLoops` provides matrix elements for arbitrary standard model processes in LO as well as NLO QCD and EW corrections. The goal of this thesis was to add the EW Sudakov approximation. Since the Sudakov approximation only relies on leading order matrix elements, it is computationally much cheaper than the rather complex full EW correction, especially for final states involving many particles.

The matrix element including the NLO correction looks like

$$|\mathcal{M}|^2_{\text{NLO}} = |\mathcal{M}_0|^2 + 2\,\text{Re}(\mathcal{M}_0^* \delta\mathcal{M}). \tag{3.1}$$

The term $|\delta\mathcal{M}|^2$ already belongs to the NNLO.

The full NLO matrix element is obtained from summing over all possible helicity configurations of the external particles. Both the LO matrix elements $\mathcal{M}_0$ and the correction terms depend on the helicity (or rather the chirality in the case of the correction factors (2.5), which we can equate in the high energy limit).

Therefore we have to construct the NLO matrix element as a sum over helicity states of the external legs.

$$|\mathcal{M}|^2 = \sum_\lambda |\mathcal{M}_0(\lambda)|^2 + 2\,\text{Re}(\mathcal{M}_0(\lambda)^* \delta\mathcal{M}(\lambda)) \tag{3.2}$$

Since `OpenLoops` uses the spinor helicity formalism to construct the LO matrix elements, it internally calculates the LO matrix element $|\mathcal{M}_0(\lambda)|^2$ for a given helicity configuration λ of the external particles and then sums over all of them to obtain $|\mathcal{M}|^2$. `OpenLoops` had to be modified to make $\mathcal{M}_0(\lambda)$ available, since out of the box, it only provides $|\mathcal{M}|^2$. In addition, the bookkeeping of polarization states had to be modified in order to be able to correctly identify left- and right-chiral fermions.

It was originally planned to implement the double logarithms using the fully general formula (2.6). However, this approach eventually had to be abandoned because of difficulties encountered in correctly computing the interference terms between the leading order matrix element $\mathcal{M}_0$ and the SU(2) flipped matrix elements appearing in the correction terms.

To avoid this problem, three different approximations have been implemented to calculate the double logarithmic corrections.

The first and most naive approximation just implements formula (2.9) and ignores the angular dependent contributions from (2.12). We also neglect the mass differences between W, Z and photons thus leaving us with only the first term in the (2.9). This still includes contributions from W,Z and γ exchange but corresponds to a theory where all EW gauge boson masses equal M_W. This version of the calculation, written out in (3.3) is labeled "Sudakov no ang" in the result plots in section 4.

$$\delta^{\text{DL}}_{\text{noang}}(\lambda) = \sum_{k=1}^{N} -\frac{1}{2} C^{\text{ew}}(k, \sigma_k(\lambda)) L(s, M_W^2) \tag{3.3}$$

The arguments of C^{ew} denote the particle i and its helicity σ_i in the helicity configuration λ.

A slightly more sophisticated approach tries to approximate the angular dependent contributions by averaging over all $n(n-1)/2$ invariants $|r_{ij}|$ as in (3.4) and then use r_{avg} as the invariant in (2.6). This enables us to make use of 2.8 to obtain a single sum over external legs again, resulting in equation (3.4). This approach is labeled "Sudakov avg DL" in the plots.

$$
\begin{aligned}
r_{\text{avg}} &= \frac{2}{n(n-1)} \sum_{i=2}^{n} \sum_{j<i} |r_{ij}| \\
\delta^{\text{DL}}_{\text{avg}}(\lambda) &= \sum_{k=1}^{n} -\frac{1}{2} C^{\text{ew}}(k, \sigma_k(\lambda)) L(r_{\text{avg}}, M_W^2)
\end{aligned}
\tag{3.4}
$$

The final refinement makes sure not to include invariants associated with particles that don't couple to the electroweak force, namely gluons, and only consider invariants involved in the EW interaction. Starting out from equation (2.6), we calculate an average invariant for each external leg

$$
r_{\text{avg}}(i) = \frac{1}{n^{\text{ew}} - 1} \sum_{\substack{i<j \\ j \neq \text{gluon}}} |r_{ij}|, \tag{3.5}
$$

where n^{ew} denotes the number of external legs interacting though the EW force. Using $L(r_{\text{avg}}(k), M_W^2)$ in (2.6), we can apply (2.8) again to obtain a single sum over the external legs, this time weighted with a different double logarithm for each leg.

$$
\delta^{\text{DL}}_{\text{weighed}}(\lambda) = \sum_{k=1}^{n} -\frac{1}{2} C^{\text{ew}}(k, \sigma_k(\lambda)) L(|r_{\text{avg}}(k)|, M_W^2). \tag{3.6}
$$

This approach is labeled "Sudakov weighted DL" in the result plots.

One can prove (and it has been done in appendix E of reference [15]), that δ^{C} due to the presence of a vector boson cancels almost exactly with δ^{PR} due to the parameter c_w, the cosine of the weak mixing angle, which is the only parameter relevant to the matrix elements studied in this thesis. Thus we only implement δ^{C} due to fermions.

The operator C^{ew} is diagonal everywhere but in the neutral gauge sector. Therefore the only LO matrix element needed for W + multijet is the original matrix element $\mathcal{M}_0$. For the Z boson however, we also need the matrix element where instead of the Z, a photon is produced. To avoid the aforementioned issues with calculating interference terms between different matrix elements, the standard pp $\to \gamma$+multijet matrix element provided by `OpenLoops` was not used.

Instead, we go back to the symmetrical basis, where C^{ew} is diagonal, and additionally equals zero for the B field. The function to calculate pp $\to$ W^3+multijet was added, which is identical to the pp $\to$ Z+multijet matrix elements up to some coupling factors, which made the aforementioned technical issues disappear.

Writing the Z+multijet matrix element as

$$
\mathcal{M}_{\text{Z+jets}} = -s_w \mathcal{M}_{\text{B+jets}} + c_w \mathcal{M}_{\text{W}^3\text{+jets}} \tag{3.7}
$$

and the term common to all Sudakov approximations

$$
\begin{aligned}
C^{\text{ew}}(Z)\mathcal{M}_{\text{Z+jets}} &= -s_w C^{\text{ew}}(B)\mathcal{M}_{\text{B+jets}} + c_w C^{\text{ew}}(W^3)\mathcal{M}_{\text{W}^3\text{+jets}} \\
&= c_w C^{\text{ew}}(W^3)\mathcal{M}_{\text{W}^3\text{+jets}}
\end{aligned}
\tag{3.8}
$$

The B field did not have to be implemented, because the $C^{\text{ew}}(B) = 0$.

In the end, the implemented formulas (varying by their implementation of δ^{DL}) read

$$|\mathcal{M}|^2_{\text{NLO}} = \sum_{\lambda} \left[1 + 2\,\text{Re}(\delta^{\text{DL}}(\lambda) + \delta^{\text{C}}(\lambda) + \delta^{\text{PR}}(\lambda))\right] |\mathcal{M}_0(\lambda)|^2 \tag{3.9}$$

for W + multijet production, while for Z + multijet production we obtain

$$\begin{aligned} |\mathcal{M}|^2_{\text{NLO}} = \sum_{\lambda} &\left[1 + 2\,\text{Re}(\delta_1^{\text{DL}}(\lambda) + \delta_1^{\text{C}}(\lambda) + \delta_1^{\text{PR}}(\lambda))\right] |\mathcal{M}_0(\lambda)|^2 \\ &+2\,\text{Re}(\delta_2^{\text{DL}}(\lambda))\mathcal{M}_0^*(\lambda)\mathcal{M}_{\text{W}^3+\text{jets}}(\lambda), \end{aligned} \tag{3.10}$$

where δ_1 are all diagonal and include contributions from all external legs other than the Z, while δ_2 contains the W^3 related terms described above in equation (3.8).

4. Results

4.1. General Remarks

In the following, results are presented for the processes pp $\rightarrow$ W^+ + (1 or 2) jets and pp $\rightarrow$ Z^0 + (1 or 2) jets.

All calculations were done at the current LHC collider energy of $\sqrt{s} = 13$ TeV.

The input parameters are listed in table 1. All other standard model parameters are derived from the listed parameters.

Parameter	Value
Parton distribution function	NNPDF23_nlo_as_0118_qed [18]
Mass of W boson	80.385 GeV
Mass of Z boson	91.1876 GeV
Mass of t quark	173.2 GeV
Mass of other quarks	0
Mass of Higgs boson	126 GeV
Fermi constant G_F	1.16637×10^{-5} GeV^{-2}

Table 1: Input parameters

The renormalization scale was set to

$$\frac{1}{2}\hat{H}'_T = \frac{1}{2}\sum E_T, \tag{4.1}$$

where the sum goes over the transverse energy of all final state parton level objects.

The jets were identified using `Sherpa`'s anti-k_T algorithm with the parameters $p_T^{\text{min}} = 30$ GeV, $E_T^{\text{min}} = 0$, D-parameter $= 0.4$, and $|\eta_j| < 4.5$.

Differential cross-sections with respect to the following observables have been studied:

- Pseudorapidity η of vector bosons and jets

- Transverse momentum p_T of vector bosons and jets
- Total transverse energy H_T^{tot}
- Invariant mass of the two jet system m_{jj} (two jet case only)
- Azimuth angle between jets $\Delta\phi_{12}$ (two jet case only)

The pseudorapidity η describes the angle of a particle relative to the beam axis and is defined as

$$\eta = -\ln\left(\tan\frac{\theta}{2}\right), \tag{4.2}$$

where θ is the angle between the particle three-momentum and the positive direction of the beam axis.

The transverse momentum p_T of a particle is the magnitude of the component of the particle's three-momentum that is perpendicular to the beam axis:

$$p_T = \sqrt{p_x^2 + p_y^2} \tag{4.3}$$

The total transverse energy H_T^{tot} is the sum of all parton and vector boson transverse energies, i.e.

$$H_T^{tot} = \sum_{i=1}^{n} \sqrt{p_{T,i}^2 + m_i^2} \tag{4.4}$$

In the case of two jets, we can define the invariant mass of the jet system m_{jj}:

$$m_{jj} = (E_1 + E_2)^2 - \|\mathbf{p}_1 + \mathbf{p}_2\|^2 \tag{4.5}$$

where E_i denotes the energy and $\mathbf{p}_i$ denotes the three-momentum of jet i.

The last observable, also only applicable for the multijet case, is $\Delta\phi_{12}$, thedifference of the azimuth angles $\phi_1 - \phi_2$, i.e. the angle between the transverse jet momenta.

$$\Delta\phi_{12} = \arctan\left(\frac{p_{y,1}}{p_{x,1}}\right) - \arctan\left(\frac{p_{y,2}}{p_{x,2}}\right) \tag{4.6}$$

4.1.1. Plot structure

The plots in this section are all structured identically.

The top section of the plots shows the various differential cross sections in absolute numbers.

The plot below shows the ratio between the leading order prediction and the various NLO methods.

The bottom section shows the ratio between exact NLO EW results and the three Sudakov approximations outlined in the section 3. The exact NLO EW results were provided by Jonas Lindert using the `OpenLoops`+`Sherpa` implementation described in [13].

As mentioned in section 3, infrared singularities due to massless photons are removed in a way that corresponds to using a photon-mass regulator $M_\gamma = M_W$ in the Sudakov approximation. To be consistent with this regularisation of QED singularities, in the exact NLO EW calculation we rescrict ourselves to purely virtual corrections and perform an $\overline{\text{MS}}$ subtraction of IR singularities at the scale $\mu = M_W$. In this way, the logarithms of μ^2/Q^2 that result from soft and collinear $1/\epsilon$ poles of QED origin are turned into logarithms of M_W^2/Q^2, which correspond to Sudakov logarithms from photons with $M_\gamma = M_W$.

4.2. Vector Boson + 1 jet

The integrated cross sections calculated using the various methods are displayed in table 2. As expected, the correction to the integrated cross section due to NLO EW effects is quite small. In order to see noticeable effects, one needs to look at differential cross sections.

4.2.1. Angular-dependent observables

In the case of a single jet, the angular-dependent observables studies are the pseudorapidity of the vector boson and of the jet. Since the pseudorapidity only depends on the angle and is independent of the energies of the involved particles, the correction is very small (less than 1%) and uniform across the whole range of interest.

There is no noticeable difference between the three different implementations of the Sudakov logarithms, they all result in a very small correction.

Note the almost identical shape of the distribution for the pp → W+j and the pp → Z+j process, apart from the larger overall cross section for W production.

	pp → W+j	$\sigma/\sigma_{\text{LO}}$	pp → Z+j	$\sigma/\sigma_{\text{LO}}$
LO	11498.7 pb		7065.7	
Sudakov wtd DL	11464.2 pb	−0.30%	7082.8	+0.24%
Sudakov avg DL	11549.4 pb	+0.44%	7075.6 pb	+0.14%
Sudakov no ang	11416.9 pb	−0.71%	6974.3 pb	−1.29%
NLO $\overline{\text{EW}}$	11449.5 pb	−0.43%	7011.4 pb	−1.01%

Table 2: Integrated cross sections and correction relative to LO for pp → V+jet

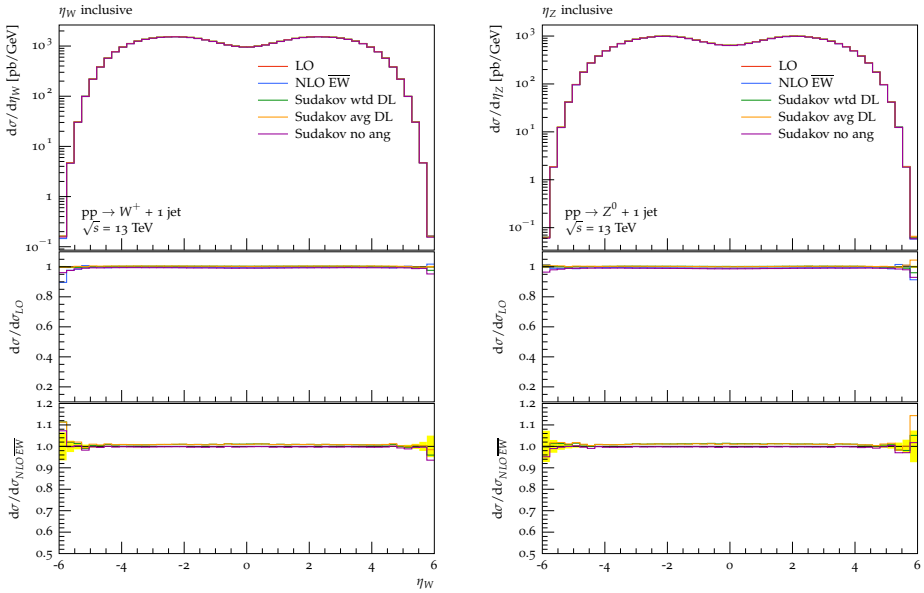

(a) η_W distribution in pp → W^++j (b) η_Z distribution in pp → Z^0+j

Figure 2: Pseudorapidity distribution of the vector boson in pp → V+j

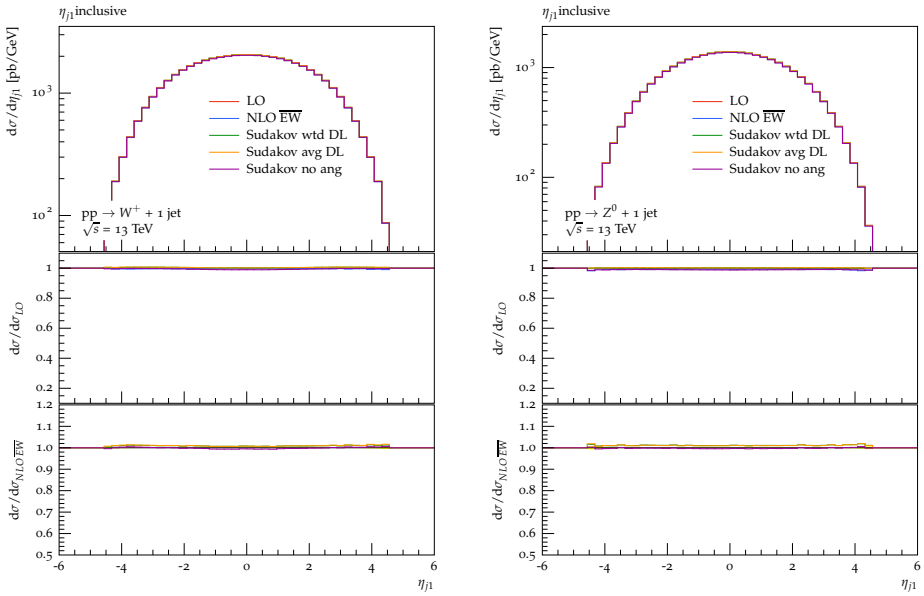

(a) η_{j1} distribution in pp → W^++j (b) η_{j1} distribution in pp → Z^0+j

Figure 3: Pseudorapidity distribution of the jet in pp → V+j

4.2.2. Energy-dependent observables

The energy dependent observables studied for the one jet case were the total transverse energy and the transverse momenta of the vector boson and jet.

For H_T^{tot} (fig. 4), the corrections are small for small values of H_T^{tot} where the cross section is the largest. For both pp $\to$ W+j (fig. 4a) and pp $\to$ Z+j (fig. 4b) they progressively increases as H_T^{tot} increases, reaching -25% for $H_T^{tot} = 2$ TeV, -40% for $H_T^{tot} = 4$ TeV, and more than -50% for $H_T^{tot} = 6$ TeV.

For the p_T distributions, we get a similar picture. First of all, the distributions in $p_{T,V}$ (fig. 5) and p_{T,j_1} (fig. 6) are virtually identical. This is of course to be expected for V + exactly one jet, since due to momentum conservation we can only produce back-to-back jets with exactly opposite transverse momenta.

As for H_T^{tot}, the (negative) corrections increase with increasing values of p_T, reaching -25% at 1 TeV and -40% at 2 TeV. Again this is not surprising, because H_T^{tot} differs from the sum of the p_T only by the vector boson mass.

Comparing the three different implementation methods, it is clear that the weighted method of (3.6) agrees the best with the full NLO $\overline{\text{EW}}$ calculation, deviating less than 2% for much of the relevant range for the W+j process and less than 4% for the Z+j process. The simple average method of (3.4) performs slightly worse, deviating around 4% for W+j and 8% for Z+j. Ignoring the angular-dependent terms is much inferior to the other two, deviating up to 20% in the same range for both processes.

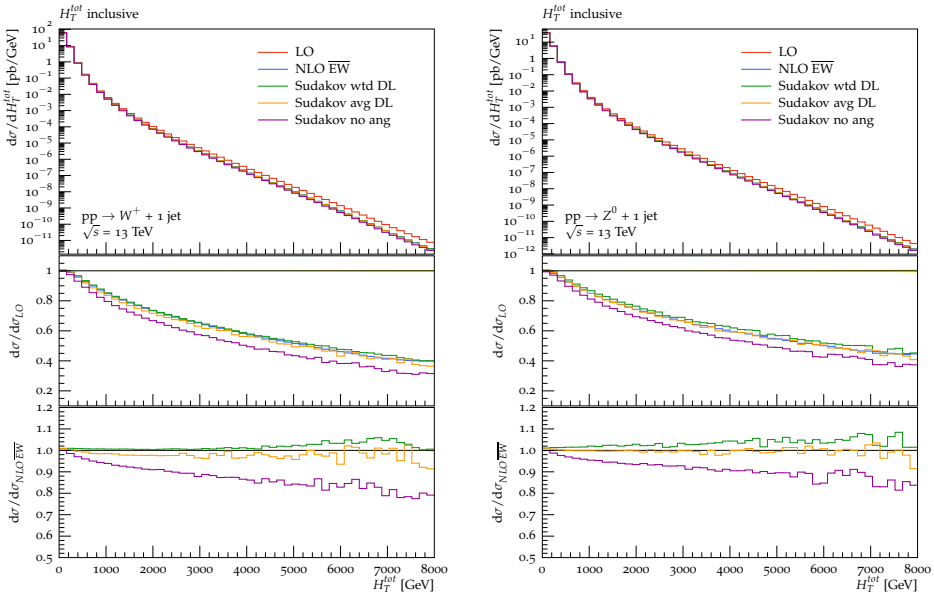

(a) H_T^{tot} distribution in pp → W^++j (b) H_T^{tot} distribution in pp → Z^0+j

Figure 4: Total transverse energy distribution in pp → V+j

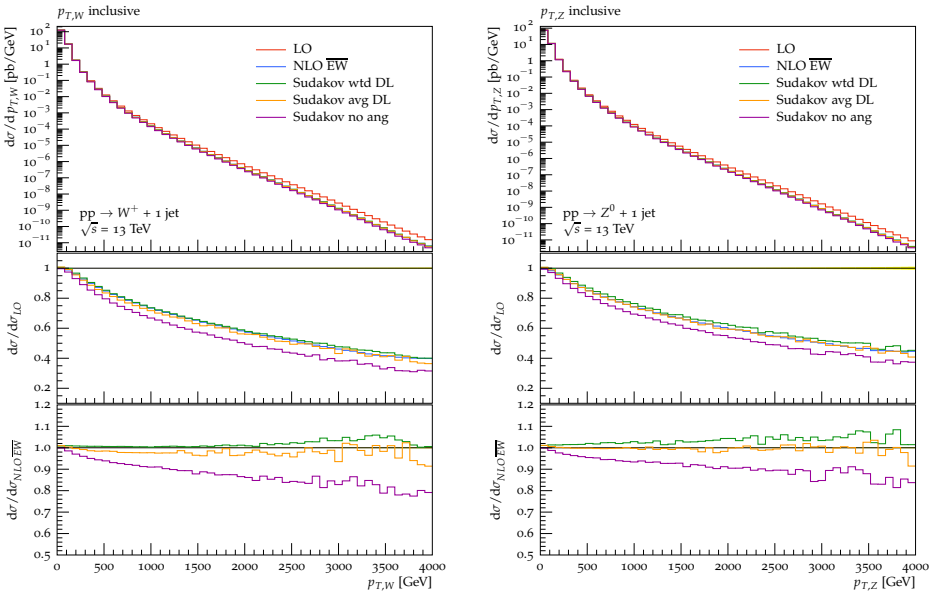

(a) $p_{T,W}$ distribution in pp → W^++j (b) $p_{T,Z}$ distribution in pp → Z^0+j

Figure 5: Vector boson transverse momentum distribution in pp → V+j

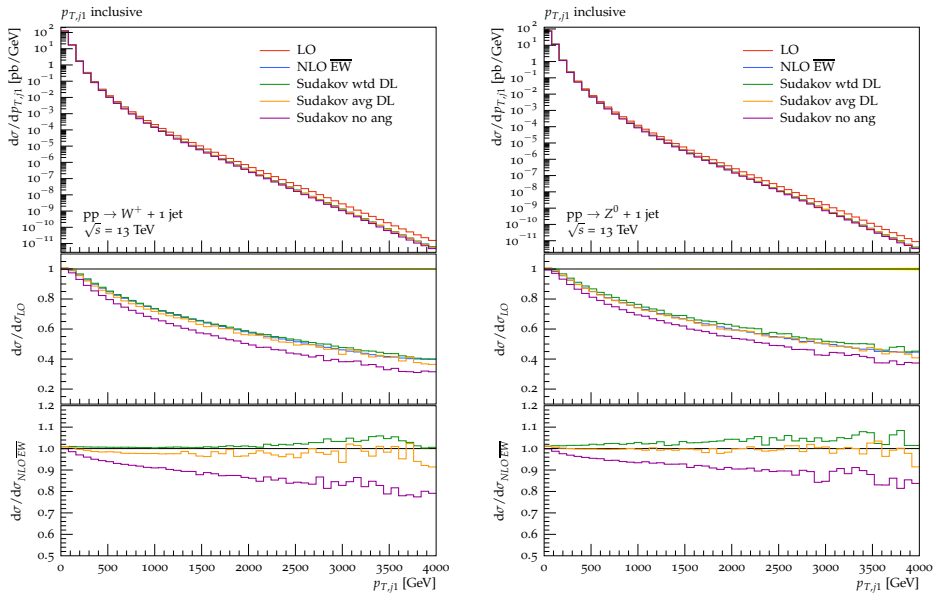

(a) $p_{T,j1}$ distribution in pp → W^++j (b) $p_{T,j1}$ distribution in pp → Z^0+j

Figure 6: Jet transverse momentum distribution in pp → V+j

4.2.3. High-energy cuts

High-energy cuts have been used to show enhanced effects of the Sudakov logarithms. The effects are particularly large when there is a vector boson with large transverse momentum $p_{T,V}$ involved in the process.

For V+j production, the cut applied is $p_{T,V} > 1$ TeV.

For the angular dependend observables, we still observe an almost uniform correction with the cut applied, but it is much larger at around 25% for the vector boson pseudorapidity (fig. 7), and around 30% for the jet pseudorapidity (fig. 8). In addition, the correction in not quite as flat anymore as in the inclusive case. In figure 7 there is an increase of the correction for large values of $|\eta_V|$ in all three Sudakov approximations, although it is relatively slight for the weighted approach of (3.6).

Compared to the full NLO computation, this becomes even more noticeable, as for large $|\eta_V|$ the difference in correction reaches 10% for the weighted approach and up to 25% for the other two approximations.

In the η_{j_1} distributions, this behavior is still there, but much weaker. Especially in figure 8b it can only really be seen at the very larges values of $|\eta_{j_1}|$.

We again see that the weighted DL approach results in the best agreement with the full NLO results, while ignoring the angular dependent contributions results in a significant discrepancy.

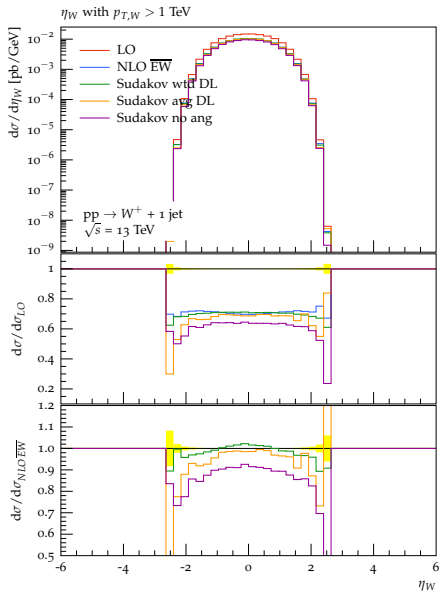

(a) η_W distribution in pp → W⁺+j with $p_{T,W} > 1$ TeV

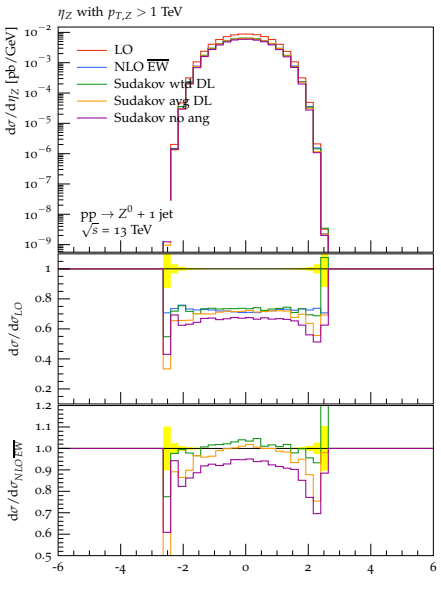

(b) η_Z distribution in pp → Z⁰+j with $p_{T,Z} > 1$ TeV

Figure 7: Pseudorapidity distribution of the vector boson in pp → V+j

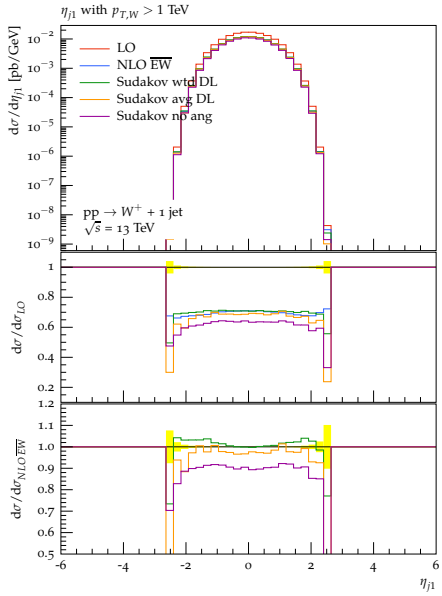

(a) η_{j1} distribution in pp → W⁺+j with $p_{T,W} > 1$ TeV

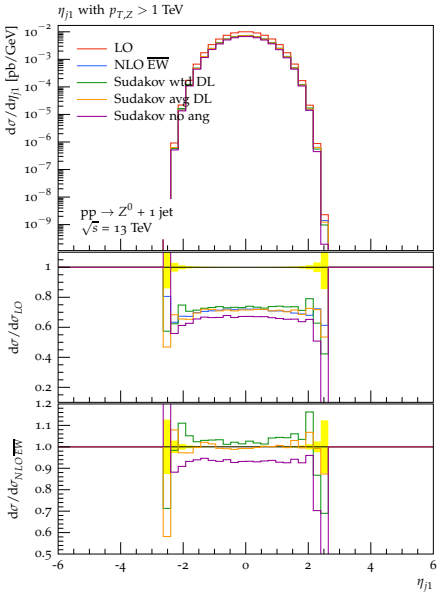

(b) η_{j1} distribution in pp → Z⁰+j with $p_{T,Z} > 1$ TeV

Figure 8: Pseudorapidity distribution of the jet in pp → V+j

4.3. Vector Boson + 2 jets

	$pp \to W^+ + 2j$	σ/σ_{LO}	$pp \to Z + 2j$	σ/σ_{LO}
LO	4012.6 pb		2363.3	
Sudakov wtd DL	3960.2 pb	−1.31%	2315.6 pb	−2.02%
Sudakov avg DL	3947.2 pb	−1.63%	2305.4 pb	−2.44%
Sudakov no ang	3770.3 pb	−6.04%	2189.1 pb	−7.37%
NLO $\overline{\text{EW}}$	3979.2 pb	−0.8%	2330.9 pb	−1.37%

Table 3: Integrated cross sections for pp → V+2 jets

The integrated cross section results are summarized in table 3. Compared to the V+jet results in table 2, the corrections to the integrated cross sections are a bit larger, but still on the order of a few percent. Again, the significant corrections show up in the differential cross sections where p_T is large.

4.3.1. Angular-dependent observables

The angular dependent observables again show very small corrections only. As for V+j, we can study the pseudorapidity of the vector boson (fig. 9) and of the the first jet (fig. 10). The corrections remain small, but instead of the almost perfectly flat distribution of the corrections for V+j, we now notice an increase of the corrections for large $|\eta_V|$ as in the V+j with high energy cuts applied, although the effect is much smaller here, only reaching a maximum difference of about 5% in all but the "no angular" approximations. In the η_{j_1} distribution, this effect is barely there at all. There is no significant difference between W and Z production here.

In addition, we now can also study the second jet (fig. 11) and the azimuth angle between the jets (fig. 12).

The η_{j_2} distribution looks virtually identical to the η_{j_1} distribution, which is not that surprising.

The $\Delta\phi_{12}$ distribution shows very small corrections compared to LO in all the considered approaches, about 5% for the "no ang" approach and around 1% for the other two. It is almost completely flat across the whole range of $\Delta\phi_{12} = 0$ to $\Delta\phi_{12} = \pi$. Only the "no ang" approach shows a slight increase for larger angles.

Interestingly, the full NLO calculation here agrees better with the "no ang" approach than the other two.

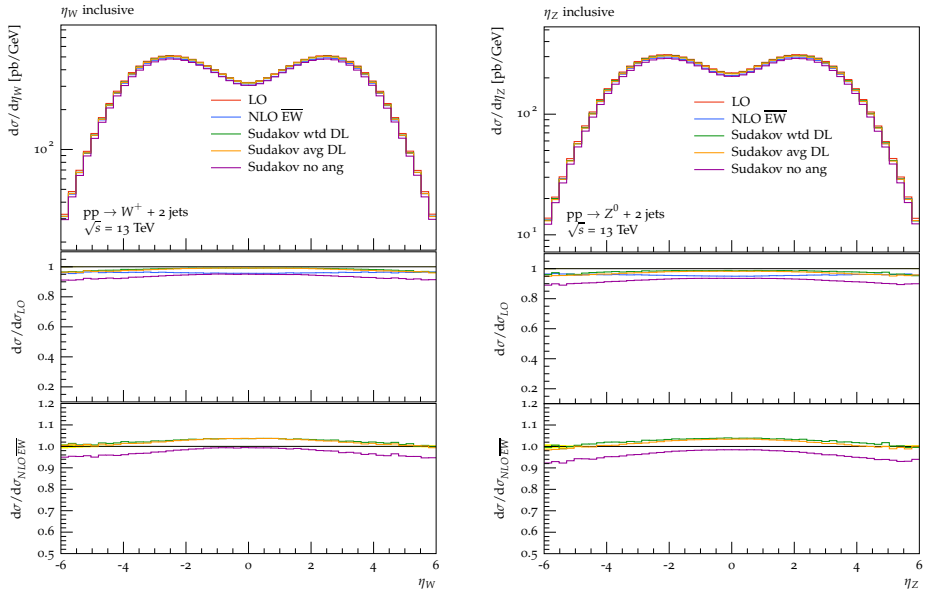

(a) η_W distribution in pp → W^++2j (b) η_Z distribution in pp → Z^0+2j

Figure 9: Pseudorapidity distribution of the vector boson in pp → V+2j

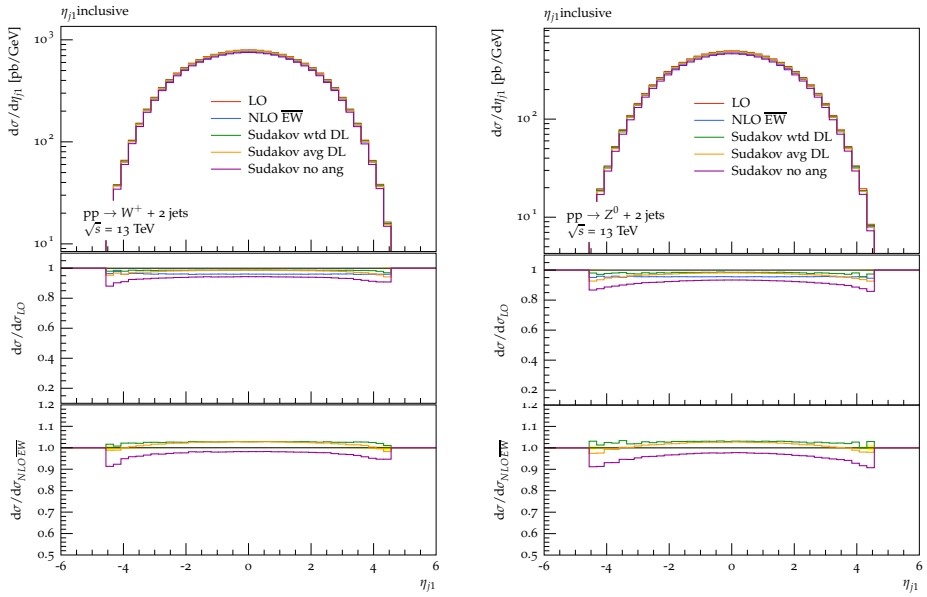

(a) η_{j1} distribution in pp → W^++2j (b) η_{j1} distribution in pp → Z^0+2j

Figure 10: Pseudorapidity distribution of the first jet in pp → V+2j

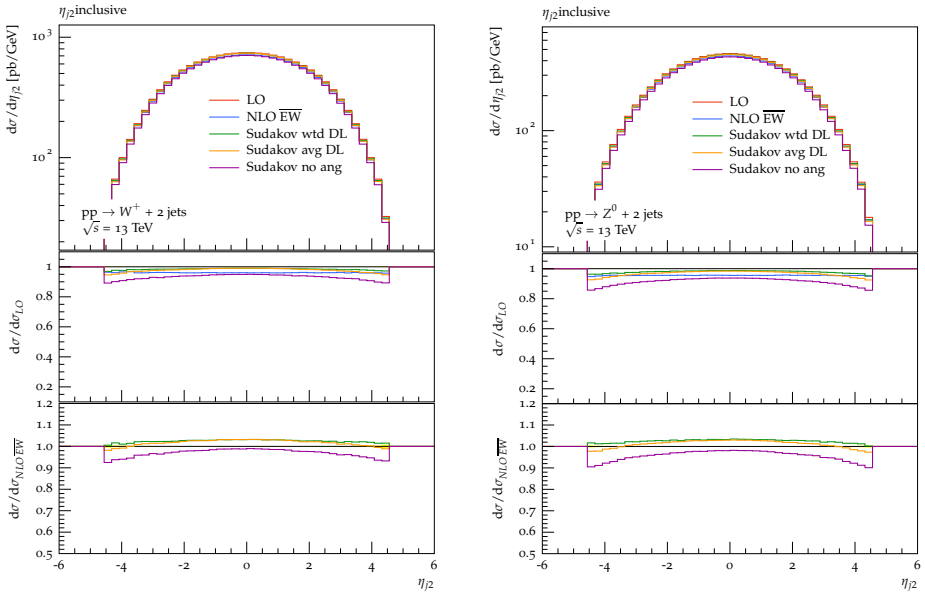

(a) η_{j2} distribution in pp → W^++2j (b) η_{j2} distribution in pp → Z^0+2j

Figure 11: Pseudorapidity distribution of the second jet in pp → V+2j

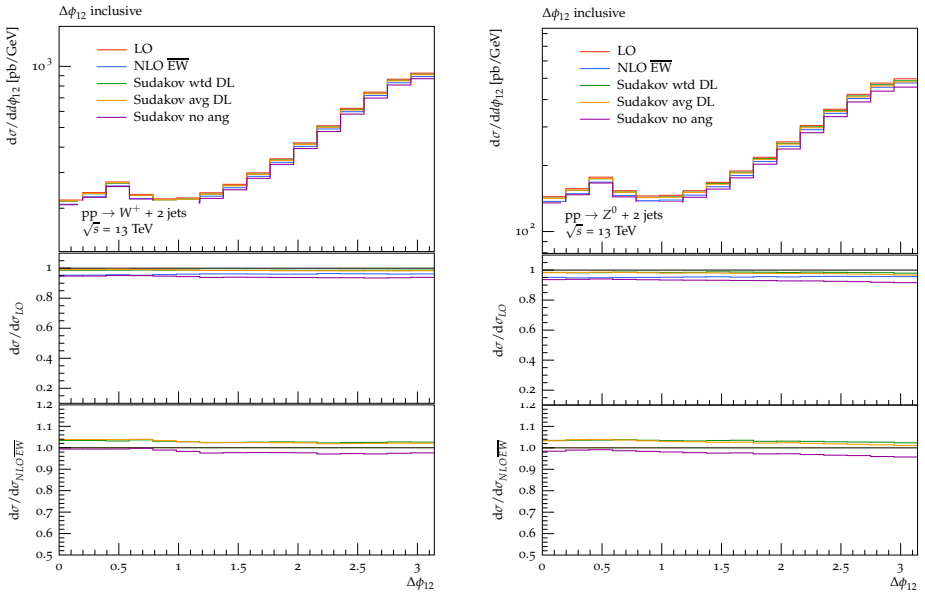

(a) $\Delta\phi_{12}$ distribution in pp → W^++2j (b) $\Delta\phi$12 distribution in pp → Z^0+2j

Figure 12: Distribution of the angle between the two jets in pp → V+2j

4.3.2. Energy-dependent observables

The inclusive energy-dependent observables studied already for V+j already are H_T^{tot}, $p_{T,V}$ and p_{T,j_1}.

For the H_T^{tot} distribution (fig. 13), the corrections have decreased significantly, only -15% at 2 TeV and -30% at 6 TeV as compared to -25% and -50%, respectively, for V+j. Other than that, the structure of the corrections remain the same, continually increasing with increasing H_T^{tot}. Note the enormous discrepancy between the "no ang" approximation and al the others. It seems the angular dependent log terms make up a larger fraction of the correction here than with most other observables.

The $p_{T,V}$ distribution (fig. 14) is virtually identical to the V+j case.

In the p_{T,j_1} distribution (fig. 15) we notice a decrease in the size of the correction compared to the V+j case. At 1 TeV, corrections reach -15% as compared to -25%, and around -30% instead of -50% in V+j. This is due to the fact that the p_{T,j_1} is not necessarily accompanied by an equally large $p_{T,V}$ but is also compensated by the second jet. This shows again that a large $p_{T,V}$ leads to larger corrections.

The p_{T,j_2} distribution in (fig. 16) looks very similar to the p_{T,j_1} case, with just slightly smaller corrections.

At V+2j, we can also look at the invariant mass of the two jets m_{jj} (fig. 17). This is the only observable studied where the Sudakov approximation does not appear to work particularly well. The slight incerase in correction shown in the full NLO calculation is strongly enhanced in the Sudakov approximation, reaching a difference of 10-15% for much of the studied range in the best case and almost 50% in the case of the "no ang" approximation. This is most likely due to the condition (2.3) not being fulfilled in a consistent manner for large values of m_{jj}.

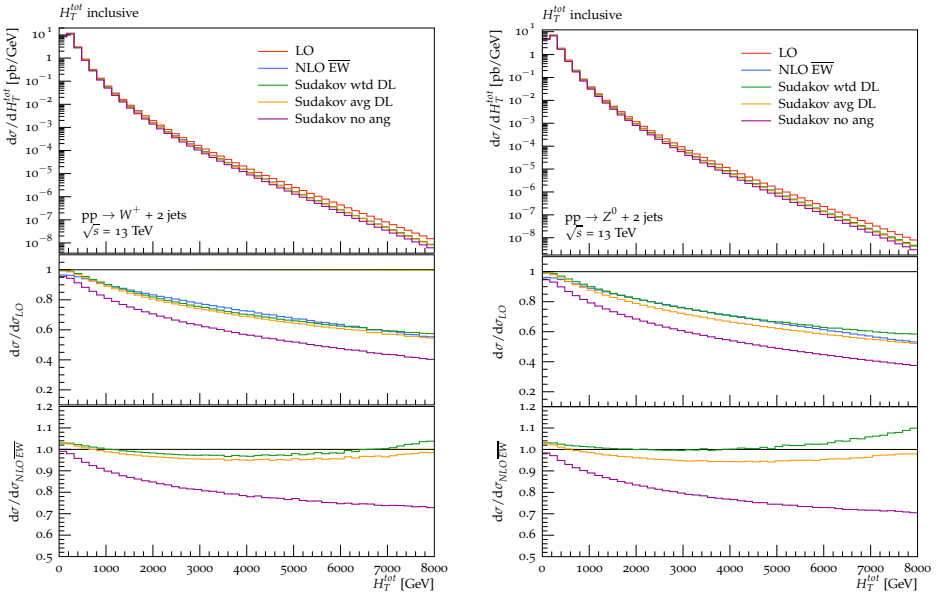

(a) H_T^{tot} distribution in pp → W$^+$+2j (b) H_T^{tot} distribution in pp → Z^0+2j

Figure 13: Total transverse energy distribution in pp → V+2j

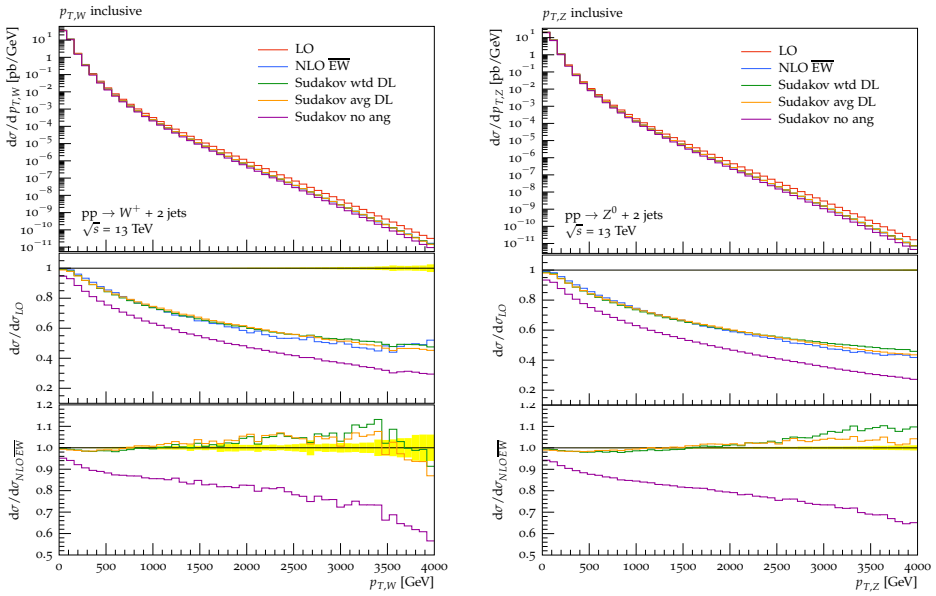

(a) $p_{T,W}$ distribution in pp → W$^+$+2j (b) $p_{T,Z}$ distribution in pp → Z^0+2j

Figure 14: Vector boson transverse momentum distribution in pp → V+2j

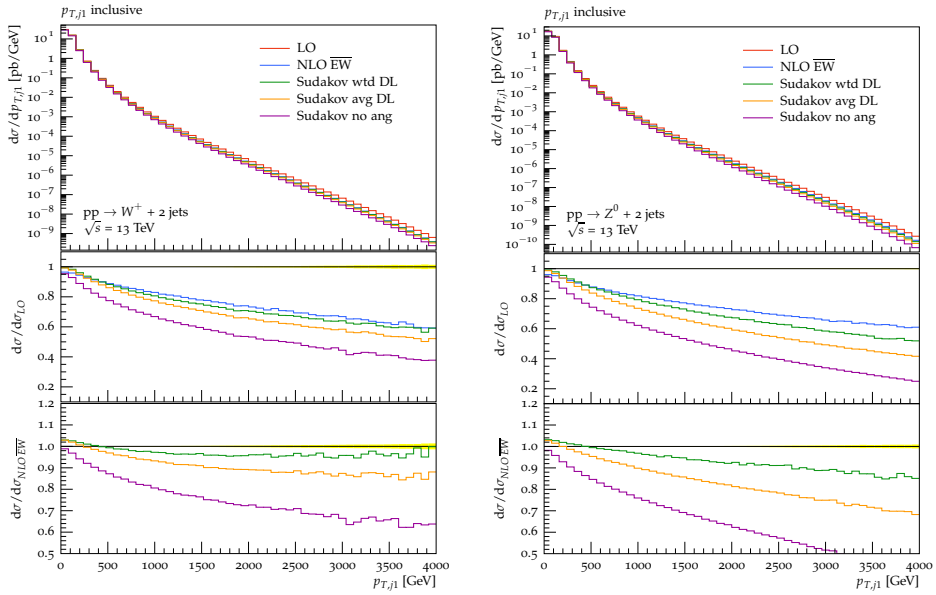

(a) $p_{T,j1}$ distribution in pp → W^++2j (b) $p_{T,j1}$ distribution in pp → Z^0+2j

Figure 15: Distribution of the transverse momentum of the first jet in pp → V+2j

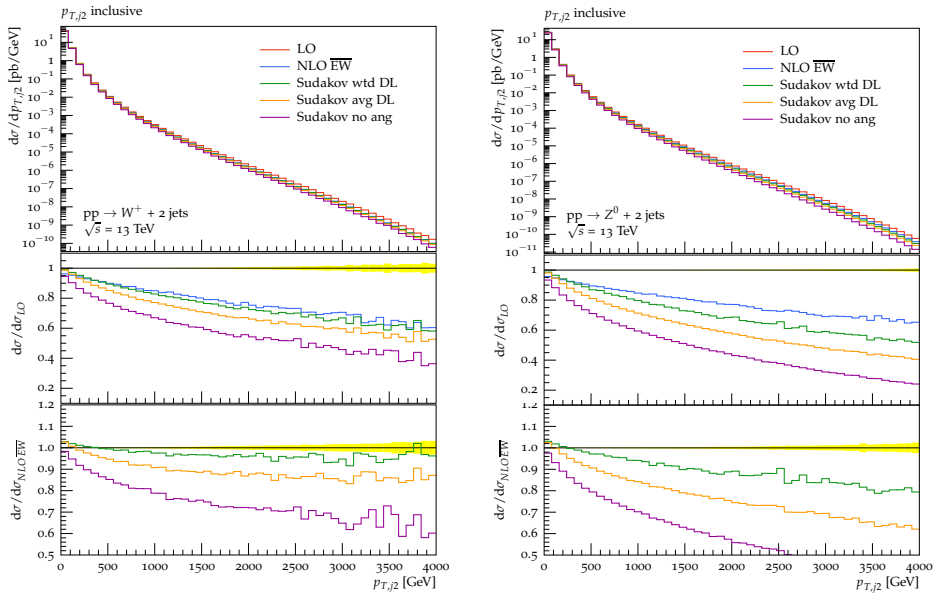

(a) $p_{T,j2}$ distribution in pp → W^++2j (b) $p_{T,j2}$ distribution in pp → Z^0+2j

Figure 16: Distribution of the transverse momentum of the second jet in pp → V+2j

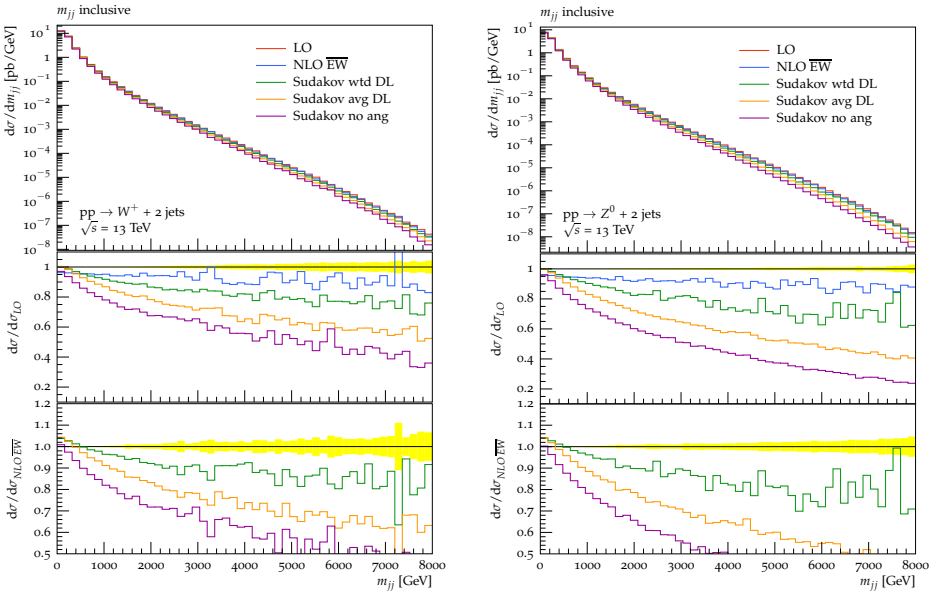

(a) m_{jj} distribution in pp → W$^+$+2j (b) m_{jj} distribution in pp → Z^0+2j

Figure 17: Two jet invariant mass distribution in pp → V+2j

4.3.3. High-energy cuts

As in the one jet case, high-energy cuts have been used to show enhanced effects of the Sudakov logarithms.

In addition to the $p_{T,V} > 1$ TeV cut introduced in section 4.2, in the case of two jets, we can also require $\Delta\phi_{12} < 3\pi/4$. This makes sure that the conservation of momentum in the transverse plane is not fulfilled by back-to-back hard jets and a soft vector boson. Instead, it requires that the sum of the jet momenta leaves the vector boson with a considerable amount of transverse momentum to absorb. However, it does allow for much softer gauge boson transverse momenta.

The effect of the cut on the η distributions (fig. 18, 19 and 20) have already been discussed in section 4.2.3 and appear virtually unchanged in V+2j.

The only interesting feature shows up in the distribution of η_{j_2} in figure 20, where applying the cut changes the shape of the distribution away from allowing a relatively wide range of η to strongly preferring $|\eta|$ around 0. However, this effect already shows up in LO and the corrections look identical to the previously discussed η distributions.

The last angular-dependent observable $\Delta\phi_{12}$ (fig. 21) shows strongly enhanced corrections of -30% across the whole range.The effect is evenly distributed and does not show any unexpected features.

Applying the $\Delta\phi_{12} < 3\pi/4$ cut on the H_T^{tot} distribution (fig. 22) only enhances the correction by a few percent compared to the inclusive distribution in figure 13.

The m_jj distribution (fig. 23) behaves similarly to the angular dependend observables. The corrections are enhanced across the whole range by around -30%, while the overall shape of the corrections remains the same.

Applying the $p_{T,V} > 1$ TeV cut to the $p_{T,j1}$ distributions (fig. 24) changes the shape of the distribution to one peaked at $p_{T,j1} = 1$ TeV with a sharp cut-off at 500 GeV. It is also around this peak that we notice the strongest enhancement of the corrections (increasing from -15% to more than -25%, with the tail end only slightly affected.

The second jet is less affected by the cut, but still the area of low p_{T,j_2} experiences a strong enhancement of the correction to around -30%.

The effect of the $\Delta\phi_{12}$ cut on the $p_{T,j}$ distributions (fig. 26 and 27) more subtle and appear to have an almost negligable effect on the cross section.

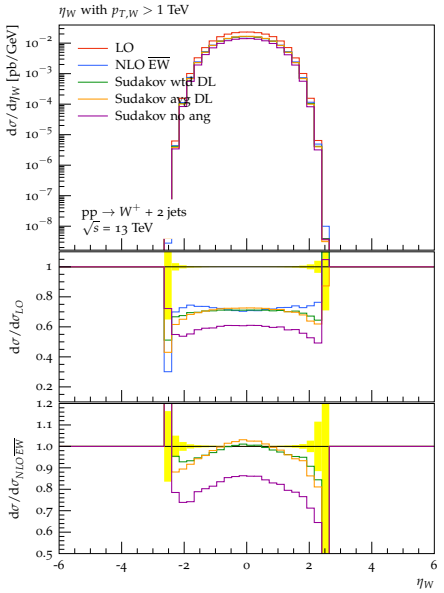

(a) η_W distribution in pp $\rightarrow$ W$^+$+2j with $p_{T,W} > 1$ TeV

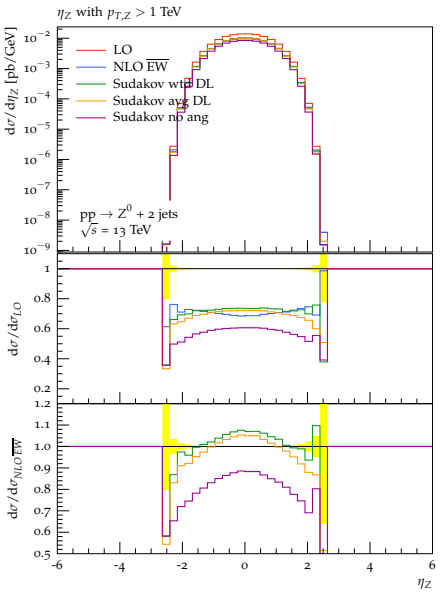

(b) η_Z distribution in pp $\rightarrow$ Z^0+2j with $p_{T,Z} > 1$ TeV

Figure 18: Pseudorapidity distribution of the vector boson in pp $\rightarrow$ V+2j with $p_{T,V} > 1$ TeV

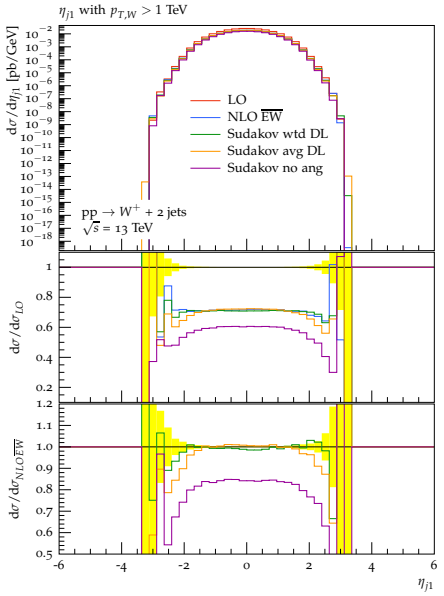

(a) η_{j1} distribution in pp $\rightarrow$ W$^+$+jet with $p_{T,W} > 1$ TeV

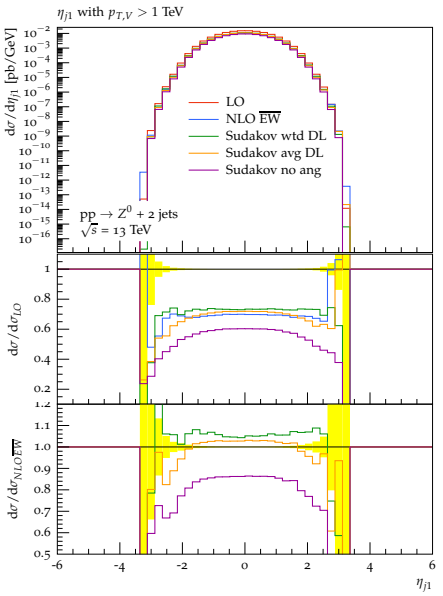

(b) η_{j1} distribution in pp $\rightarrow$ Z^0+2j with $p_{T,Z} > 1$ TeV

Figure 19: Pseudorapidity distribution of the first jet in pp $\rightarrow$ V+2j with $p_{T,V} > 1$ TeV

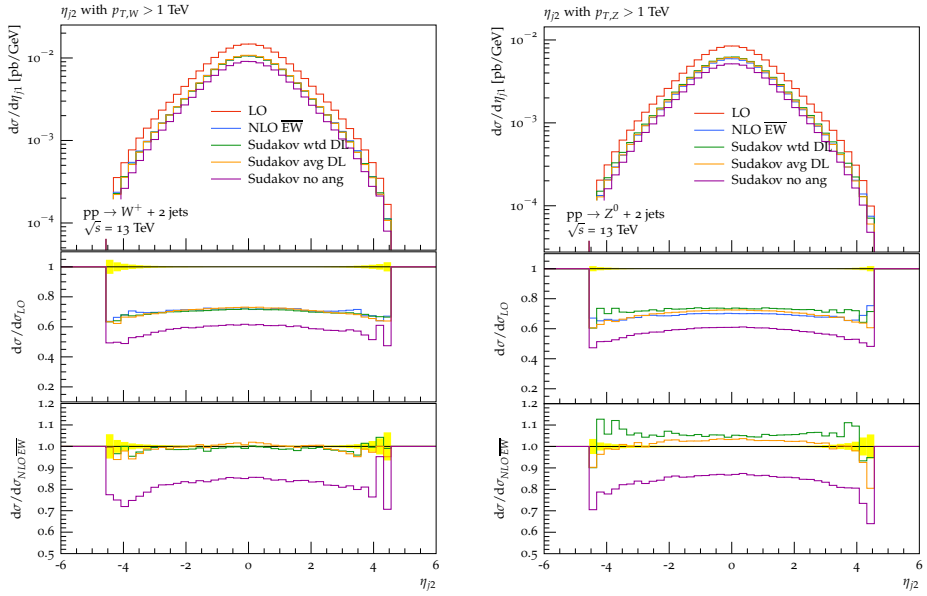

(a) η_{j2} distribution in pp $\rightarrow$ W$^+$+jet with $p_{T,W} > 1$ TeV

(b) η_{j2} distribution in pp $\rightarrow$ Z^0+2j with $p_{T,Z} > 1$ TeV

Figure 20: Pseudorapidity distribution of the second jet in pp $\rightarrow$ V+2j with $p_{T,V} > 1$ TeV

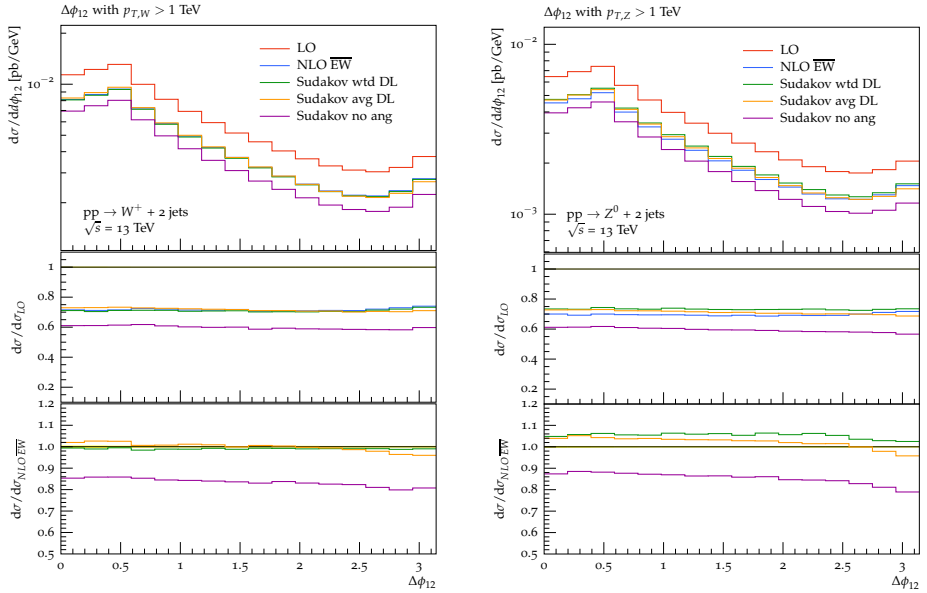

(a) $\Delta\phi_{12}$ distribution in pp $\rightarrow$ W$^+$+2j with $p_{T,W} > 1$ TeV

(b) $\Delta\phi$12 distribution in pp $\rightarrow$ Z^0+2j with $p_{T,Z} > 1$ TeV

Figure 21: Distribution of the angle between the two jets in pp $\rightarrow$ V+2j with $p_{T,V} > 1$ TeV

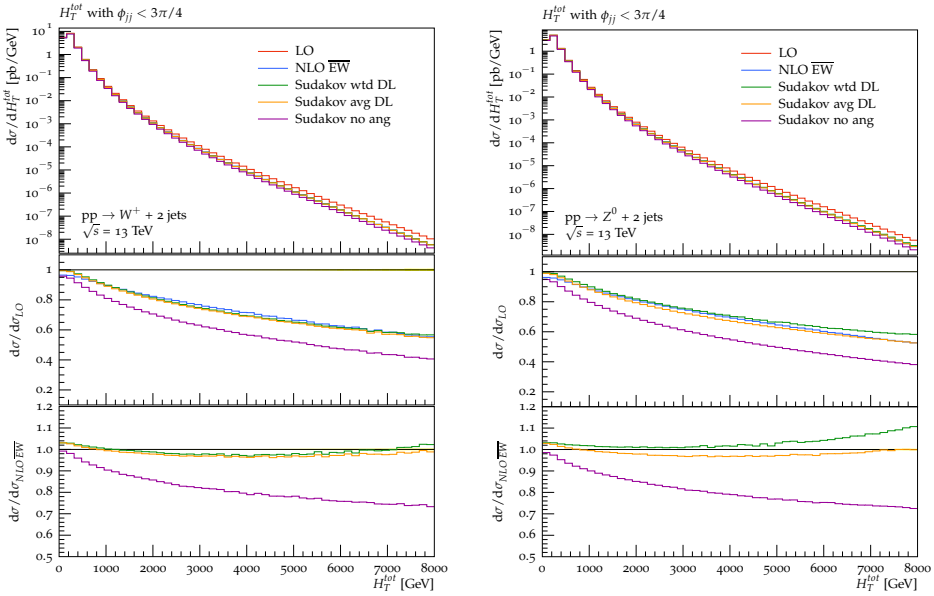

(a) H_T^{tot} distribution in pp → W$^+$+2j with $\Delta\phi_{12} < 3\pi/4$

(b) H_T^{tot} distribution in pp → Z^0+2j with $p_{T,Z} > 1$ TeV

Figure 22: Total transverse energy distribution in pp → V+2j with $\Delta\phi_{12} < 3\pi/4$

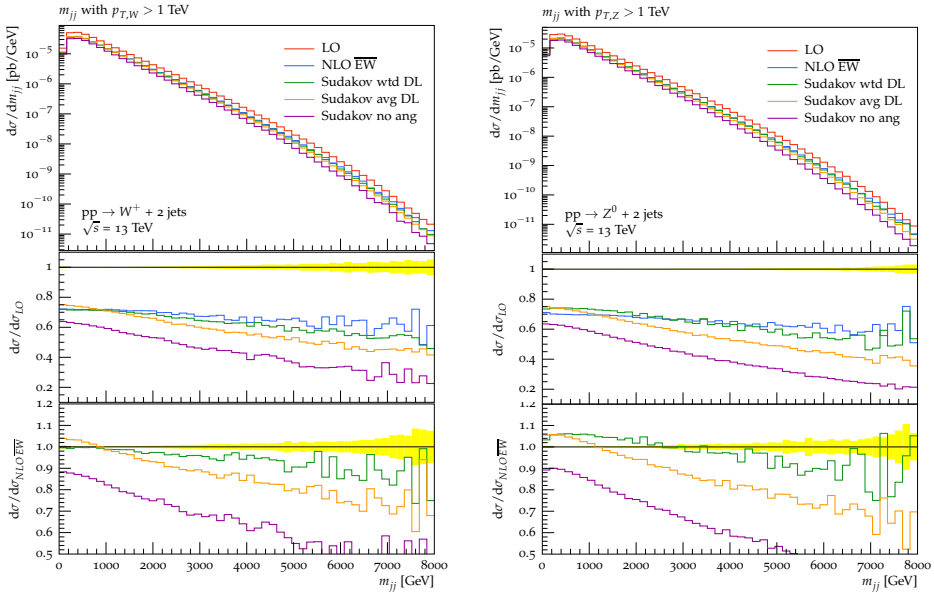

(a) m_{jj} distribution in pp → W$^+$+2j with $p_{T,W} > 1$ TeV

(b) m_{jj} distribution in pp → Z^0+2j with $p_{T,Z} > 1$ TeV

Figure 23: Two jet invariant mass distribution in pp → V+2j with $p_{T,V} > 1$ TeV

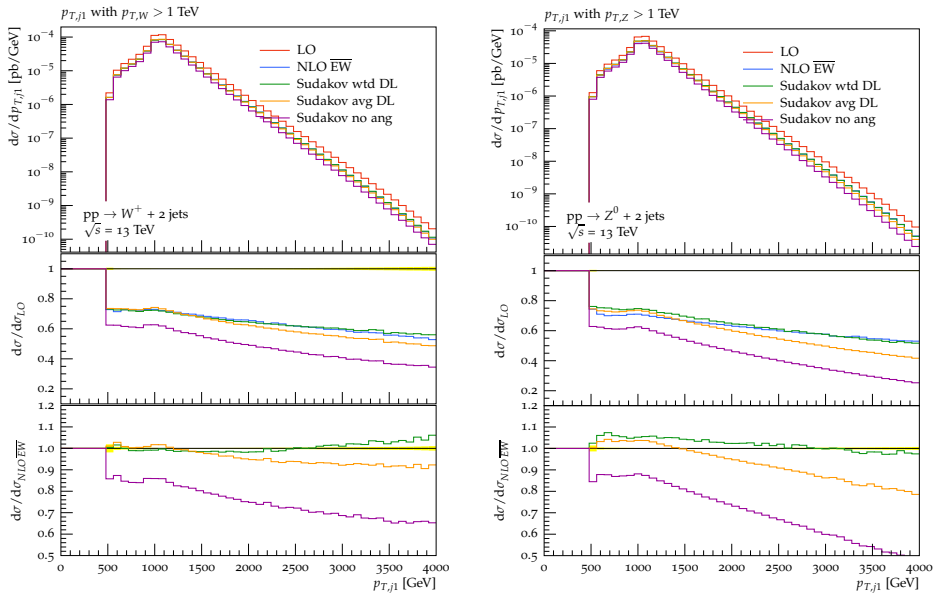

(a) $p_{T,j1}$ distribution in pp → W^++2j with $p_{T,W} > 1$ TeV

(b) $p_{T,j1}$ distribution in pp → Z^0+2j with $p_{T,Z} > 1$ TeV

Figure 24: Distribution of the transverse momentum of the first jet in pp → V+2j with $p_{T,V} > 1$ TeV

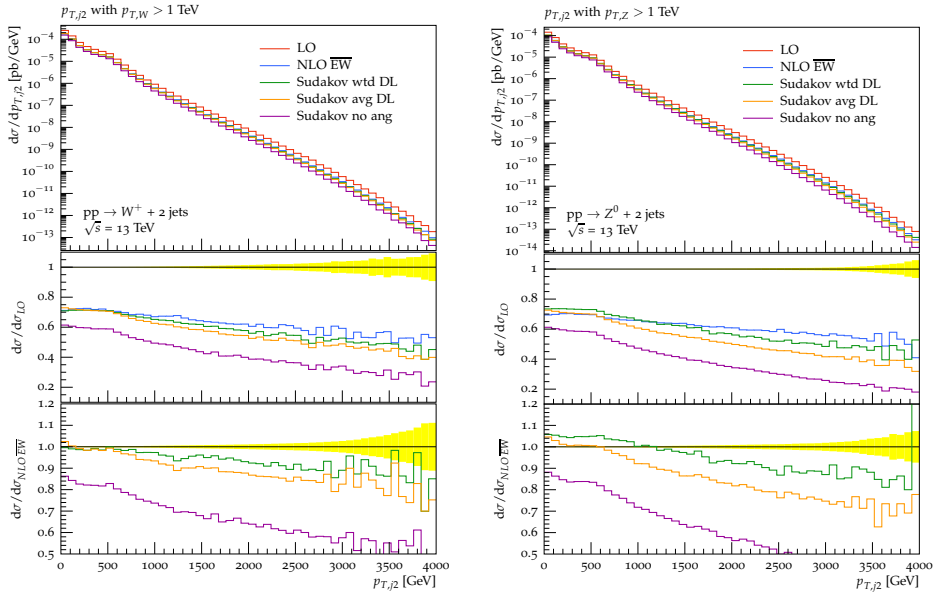

(a) $p_{T,j2}$ distribution in pp → W^++2j with $p_{T,W} > 1$ TeV

(b) $p_{T,j2}$ distribution in pp → Z^0+2j with $p_{T,Z} > 1$ TeV

Figure 25: Distribution of the transverse momentum of the second jet in pp → V+2j with $p_{T,V} > 1$ TeV

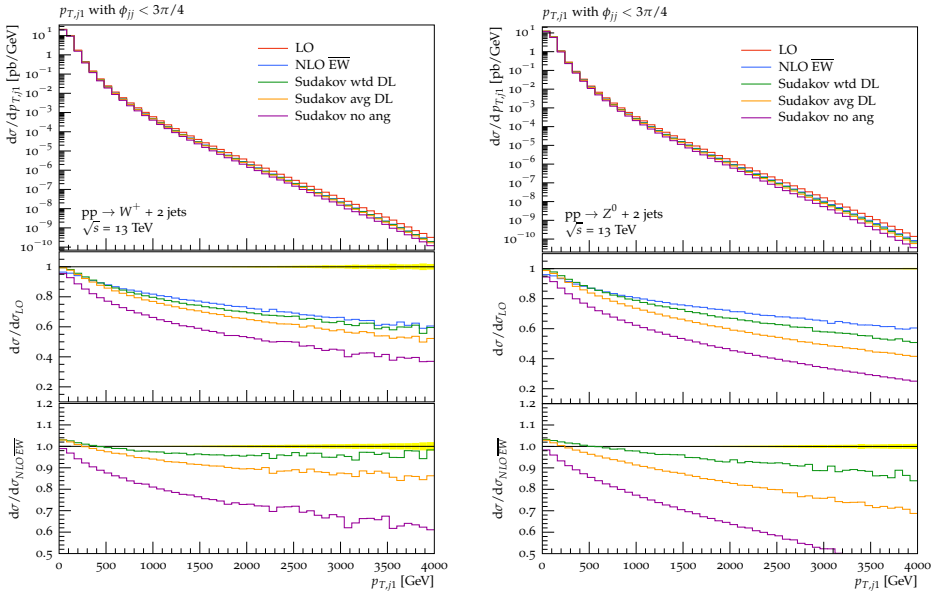

(a) $p_{T,j1}$ distribution in pp → W$^+$+2j with $\Delta\phi_{12} < 3\pi/4$

(b) $p_{T,j1}$ distribution in pp → Z^0+2j with $\Delta\phi_{12} < 3\pi/4$

Figure 26: Distribution of the transverse momentum of the first jet in pp → V+2j with $\Delta\phi_{12} < 3\pi/4$

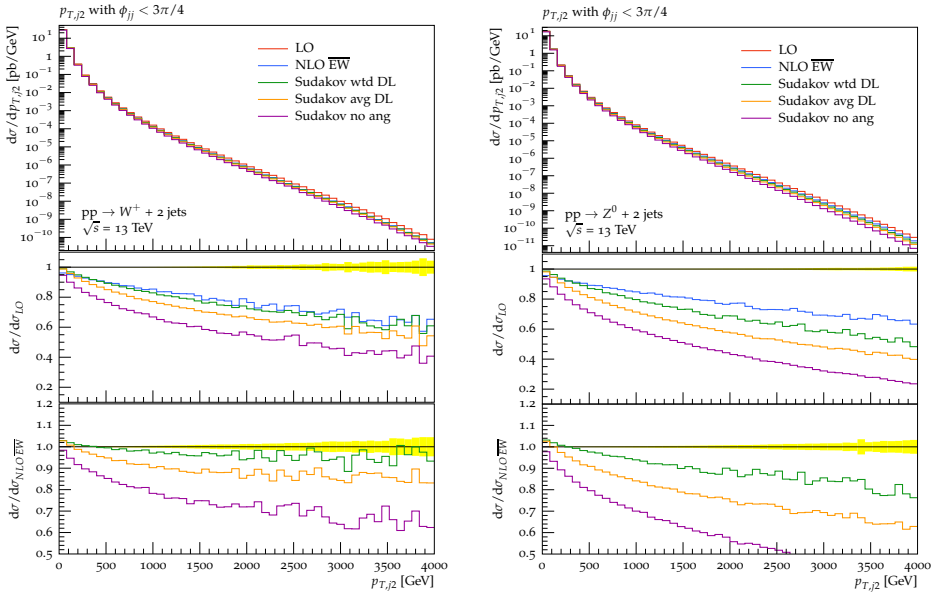

(a) $p_{T,j2}$ distribution in pp → W$^+$+jet with $p_{T,W} > 1$ TeV

(b) $p_{T,j2}$ distribution in pp → Z^0+2j with $p_{T,Z} > 1$ TeV

Figure 27: Distribution of the transverse momentum of the second jet in pp → V+2j with $\Delta\phi_{12} < 3\pi/4$

5. Summary and Conclusions

We implemented the Sudakov logarithms approximation to the electroweak next-to-leading order corrections to the process pp $\to$ V + j.

The corrections were implemented in the `OpenLoops` matrix element generator and used the `Sherpa` Monte Carlo generator to generate the hadron collider simulations.

The double logarithms were implemented in three different approximations, where the weighted approach described in equation (3.6) proved most accurate.

The results showed large corrections of up to 50% occurring whenever the transverse momentum of the gauge boson was large. This is an important effect that needs to be included in order to get accurate predictions for V+jets.

The agreement between the Sudakov logarithms and the exact NLO EW calculation was very good in most cases. For most observables the deviation was less than 5% for much of the studied range. The main exception was the m_{jj} observable, the invariant jet mass of the two jet system in pp $\to$ V + 2 jets, where the Sudakov approximations significantly overestimated the corrections as compared to the exact calculations.

A future implementation should attempt to keep track of the degree to which the preconditions that make the Sudakov appriximation accurate are met.

Overall, the Sudakov approximation proved very effective and should be implemented in a fully general, automatic manner and be validated more extensively. Then it could prove to be a very useful tool for processes involving many particles in the final state, as the computational complexity is the same as for leading order matrix elements.

A. Operators and their eigenvalues

For the production of Z bosons, both the symmetrical and the physical basis of the gauge bosons were used.

The physical fields $N = A, Z$ are related to the symmetrical fields $\tilde{N} = B, W^3$ through the Weinberg rotation,

$$N = U_{N\tilde{N}}(\theta_w)\tilde{N}, \qquad U(\theta_w = \begin{pmatrix} c_w & -s_w \\ s_w & c_w \end{pmatrix} \tag{A.1}$$

where $c_w = \cos\theta_w$ and $s_w = \sin\theta_w$. The weak mixing angle is fixed by

$$c_w = \frac{M_W}{M_Z}. \tag{A.2}$$

The gauge couplings in the symmetrical basis read

$$\tilde{I}^B = -\frac{1}{c_w}\frac{Y}{2}, \qquad \tilde{I}^{W^a} = \frac{1}{s_w}T^a, \qquad a = 1, 2, 3 \tag{A.3}$$

where Y denotes the weak hypercharge and T^a are the components of the weak isospin. In the physical basis this results in

$$I^A = -Q, \quad I^Z = \frac{T^3 - s_w^2 Q}{s_w c_w}, I^{\pm} = \frac{1}{s_w}T^{\pm} = \frac{1}{s_w}\frac{T^1 \pm \mathrm{i}T^2}{\sqrt{2}} \tag{A.4}$$

with $Q = T^3 + Y/2$.

The electroweak Casimir operator is

$$C^{\mathrm{ew}} := \sum_{V_a = A,Z,W^{\pm}} I^{V^a} I^{\bar{V}^a}. \tag{A.5}$$

In table 4, explicit values of operator eigenvalues used in the implemented processes are given.

EW β-function

The one-loop coefficients of the β-function in the symmetric basis are

$$\tilde{b}_B^{\mathrm{ew}} = -\frac{41}{6c_w^2}, \qquad \tilde{b}_W^{\mathrm{ew}} = \frac{19}{6s_w^2}. \tag{A.6}$$

In the physical basis, they become

$$\begin{aligned} b_{AA}^{\mathrm{ew}} &= -\frac{11}{3} \\ b_{AZ}^{\mathrm{ew}} &= -\frac{19 + 22s_w^2}{6s_w c_w} \\ b_{ZZ}^{\mathrm{ew}} &= -\frac{19 - 38s_w^2 - 22s_w^4}{6s_w c_w}. \end{aligned} \tag{A.7}$$

	$Y/2$	Q	T^3	$(I^A)^2$	$(I^Z)^2$	$(I^W)^2$	C^{ew}
u^{L}, $\bar{u}^{\mathrm{L}}$	$\pm\frac{1}{6}$	$\pm\frac{2}{3}$	$\pm\frac{1}{2}$	$\frac{4}{9}$	$\frac{(3c_w^2-s_w^2)^2}{36s_w^2c_w^2}$	$\frac{1}{2s_w^2}$	$\frac{s_2^2+27c_w^2}{36c_w^2s_w^2}$
d^{L}, $\bar{d}^{\mathrm{L}}$	$\pm\frac{1}{6}$	$\mp\frac{1}{3}$	$\mp\frac{1}{2}$	$\frac{1}{9}$	$\frac{(3c_w^2+s_w^2)^2}{36s_w^2c_w^2}$	$\frac{1}{2s_w^2}$	$\frac{s_2^2+27c_w^2}{36c_w^2s_w^2}$
u^{R}, $\bar{u}^{\mathrm{R}}$	$\pm\frac{2}{3}$	$\pm\frac{2}{3}$	0	$\frac{4}{9}$	$\frac{4}{9}\frac{s_w^2}{c_w^2}$	0	$\frac{4}{9c_w^2}$
d^{R}, $\bar{d}^{\mathrm{R}}$	$\mp\frac{1}{3}$	$\mp\frac{1}{3}$	0	$\frac{1}{9}$	$\frac{1}{9}\frac{s_w^2}{c_w^2}$	0	$\frac{1}{9c_w^2}$
$W^{\pm}$	0	±1	±1	1	$\frac{c_w^2}{s_w^2}$	$\frac{1}{s_w^2}$	$\frac{2}{s_w^2}$
W^3	0	0	0	0	0	$\frac{2}{s_w^2}$	$\frac{2}{s_w^2}$
B	0	0	0	0	0	0	0

Table 4: SU(2) operator eigenvalues

References

[1] Georges Aad et al. "Measurement of the production cross section for W-bosons in association with jets in pp collisions at $\sqrt{s} = 7$ TeV with the ATLAS detector". In: *Phys. Lett.* B698 (2011), pp. 325–345. DOI: 10.1016/j.physletb.2011.03.012. arXiv: 1012.5382 [hep-ex].

[2] Georges Aad et al. "Study of jets produced in association with a W boson in pp collisions at $\sqrt{s} = 7$ TeV with the ATLAS detector". In: *Phys. Rev.* D85 (2012), p. 092002. DOI: 10.1103/PhysRevD.85.092002. arXiv: 1201.1276 [hep-ex].

[3] Georges Aad et al. "Measurements of the W production cross sections in association with jets with the ATLAS detector". In: *Eur. Phys. J.* C75.2 (2015), p. 82. DOI: 10.1140/epjc/s10052-015-3262-7. arXiv: 1409.8639 [hep-ex].

[4] Serguei Chatrchyan et al. "Jet Production Rates in Association with W and Z Bosons in pp Collisions at $\sqrt{s} = 7$ TeV". In: *JHEP* 01 (2012), p. 010. DOI: 10.1007/JHEP01(2012)010. arXiv: 1110.3226 [hep-ex].

[5] Serguei Chatrchyan et al. "Study of the dijet mass spectrum in $pp \to W+$ jets events at $\sqrt{s} = 7$ TeV". In: *Phys. Rev. Lett.* 109 (2012), p. 251801. DOI: 10.1103/PhysRevLett.109.251801. arXiv: 1208.3477 [hep-ex].

[6] Vardan Khachatryan et al. "Differential cross section measurements for the production of a W boson in association with jets in proton–proton collisions at $\sqrt{s} = 7$ TeV". In: *Phys. Lett.* B741 (2015), pp. 12–37. DOI: 10.1016/j.physletb.2014.12.003. arXiv: 1406.7533 [hep-ex].

[7] Radja Boughezal et al. "W-boson production in association with a jet at next-to-next-to-leading order in perturbative QCD". In: *Phys. Rev. Lett.* 115.6 (2015), p. 062002. DOI: 10.1103/PhysRevLett.115.062002. arXiv: 1504.02131 [hep-ph].

[8] A. Gehrmann-De Ridder et al. "Precise QCD predictions for the production of a Z boson in association with a hadronic jet". In: (2015). arXiv: 1507.02850 [hep-ph].

[9] Stefano Actis et al. "EW and QCD One-Loop Amplitudes with RECOLA". In: *PoS* RADCOR2013 (2013), p. 034. arXiv: 1311.6662 [hep-ph].

[10] S. Actis et al. "Recursive generation of one-loop amplitudes in the Standard Model". In: *JHEP* 04 (2013), p. 037. DOI: 10.1007/JHEP04(2013)037. arXiv: 1211.6316 [hep-ph].

[11] S. Frixione et al. "Weak corrections to Higgs hadroproduction in association with a top-quark pair". In: *JHEP* 09 (2014), p. 065. DOI: 10.1007/JHEP09(2014)065. arXiv: 1407.0823 [hep-ph].

[12] Mauro Chiesa, Nicolas Greiner, and Francesco Tramontano. "Automation of electroweak corrections for LHC processes". In: *J. Phys.* G43.1 (2016), p. 013002. DOI: 10.1088/0954-3899/43/1/013002. arXiv: 1507.08579 [hep-ph].

[13] Stefan Kallweit et al. "NLO QCD+EW predictions for V+jets including off-shell vector-boson decays and multijet merging". In: (2015). arXiv: 1511.08692 [hep-ph].

[14] Fabio Cascioli, Philipp Maierhofer, and Stefano Pozzorini. "Scattering Amplitudes with Open Loops". In: *Phys. Rev. Lett.* 108 (2012), p. 111601. DOI: 10.1103/PhysRevLett.108.111601. arXiv: 1111.5206 [hep-ph].

[15] Stefano Pozzorini. "Electroweak radiative corrections at high-energies". PhD thesis. Zurich U., Inst. Math., 2001. arXiv: hep-ph/0201077 [hep-ph].

[16] T. Gleisberg et al. "Event generation with SHERPA 1.1". In: *JHEP* 02 (2009), p. 007. DOI: 10.1088/1126-6708/2009/02/007. arXiv: 0811.4622 [hep-ph].

[17] Andy Buckley et al. "Rivet user manual". In: *Comput. Phys. Commun.* 184 (2013), pp. 2803–2819. DOI: 10.1016/j.cpc.2013.05.021. arXiv: 1003.0694 [hep-ph].

[18] Richard D. Ball et al. "Parton distributions with QED corrections". In: *Nucl. Phys.* B877 (2013), pp. 290–320. DOI: 10.1016/j.nuclphysb.2013.10.010. arXiv: 1308.0598 [hep-ph].